Singlet and Triplet Energy Transfer in the Peridinin−Chlorophyll *a*−Protein from *Amphidinium carterae*

James A. Bautista,[†] Roger G. Hiller,[‡] Frank P. Sharples,[‡] David Gosztola,[§] Michael Wasielewski,[§,⊥] and Harry A. Frank*[,†]

Department of Chemistry, University of Connecticut, 55 North Eagleville Road, Storrs, Connecticut 06269-3060; School of Biological Sciences, Macquarie University, NSW 2109, Australia; Chemistry Division, Argonne National Laboratory, Argonne, Illinois 60439; and Department of Chemistry, Northwestern University, Evanston, Illinois 60208

Received: October 1, 1998; In Final Form: December 2, 1998

The spectroscopic properties of peridinin in solution, and the efficiency and dynamics of energy transfer from peridinin to chlorophyll *a* in the peridinin−chlorophyll−protein (PCP) from *Amphidinium carterae*, were studied by steady-state absorption, fluorescence, fluorescence excitation, and fast transient optical spectroscopy. Steady-state measurements of singlet energy transfer from peridinin to chlorophyll revealed an $88 \pm 2\%$ efficiency. Fast-transient absorption experiments showed that the excited S_1 state of peridinin decayed in 13.4 ± 0.6 ps in methanol and 3.1 ± 0.4 ps in the PCP complex after direct excitation of the carotenoid. The onset of the bleaching of the chlorophyll absorption band at 672 nm, signifying the arrival of the excitation from the carotenoid, occurred in 3.2 ± 0.3 ps. These data show that the primary route of energy transfer from peridinin to chlorophyll in the PCP complex is through the S_1 state of peridinin. Nanosecond time-resolved transient optical spectroscopy revealed that chlorophyll triplet states are efficiently quenched by peridinin whose triplet state subsequently decays with a lifetime of 10 ± 1 μs in the PCP complex. Close association between the peridinins and chlorophylls, which is clearly evident in the 3-D structure of the PCP complex, along with proper alignment of pigments and energy state matching are responsible for the high efficiencies of the photochemical processes.

Introduction

Photosynthetic organisms make use of discrete pigment−protein complexes for harvesting light energy and converting it into chemical potential.[1] These light-harvesting, or antenna, pigment−protein complexes are responsible for binding the vast majority of the chlorophyll (Chl) and carotenoid pigments found in nature. Several of these antenna complexes have been crystallized, and their structures have been solved to high-resolution using X-ray or electron diffraction techniques. This group of complexes consists of the LH2, or B800-850, proteins from *Rhodopseudomonas (Rps.) acidophila* strain 10050[2] and *Rhodospirillum molischianum*,[3] the LHC-II complex from higher plants,[4] the water-soluble FMO complex from *Prosthecochloris aestuarii*,[5] and the peridinin−Chl−protein (PCP) complex from the dinoflagellate, *Amphidinium carterae*.[6] The structures, pigment stoichiometries, and physical properties of these complexes vary widely, and therefore it is difficult to draw any general conclusions regarding the mechanism by which light-harvesting is accomplished. For example, the carotenoid-to-Chl stoichiometry of the LHC-II complex from higher plants is ∼2 carotenoids, most likely luteins, to 12 Chl *a* and *b* molecules.[4] In the PCP complex, the stoichiometry is 8 peridinins to 2 Chl *a* molecules.[6] These pigment stoichiometries are very different, yet both of these complexes have carotenoid-to-Chl singlet energy transfer efficiencies approaching 100%.[7,8] The LH2 complex from *Rps. acidophila* strain 10050, which has a carotenoid-to-Chl pigment stoichiometry of either 1 or 2 rhodopin glucoside molecules to 3 bacteriochlorophylls,[2] has an energy transfer efficiency of only ∼40%.[9,10] A knowledge of the molecular structures of these proteins is essential for understanding their spectroscopic properties and for building quantitative models that describe how they function as light-harvesting complexes in vivo.

In this paper, the spectroscopic properties associated with the low-lying excited states of the carotenoid, peridinin (Figure 1), in solution, and the efficiency and dynamics of energy transfer to and from peridinin and Chl *a* in the PCP complex from *Amphidinium carterae* are examined. There are two important low-lying excited singlet states of peridinin that can potentially act as energy donors to Chl. These are denoted S_1 and S_2. It is generally accepted that for polyenes and carotenoids, the S_1 state possesses A_g symmetry in the idealized C_{2h} point group.[11−13] Electronic transitions to and from S_1 and the ground state, denoted S_0, and also possessing A_g symmetry, are forbidden by symmetry; i.e. the $S_0 \rightarrow S_1$ ($1^1A_g \rightarrow 2^1A_g$) transition is forbidden. Electronic transitions to and from the S_2 state and the ground state are allowed, however, because S_2 possesses B_u symmetry in the idealized C_{2h} point group. The strong absorption in the visible region characteristic of all polyenes and carotenoids is attributable to the $S_0 \rightarrow S_2$ ($1^1A_g \rightarrow 1^1B_u$) transition. The present work addresses the issue of which of these two excited states is involved in the process of light-harvesting. In addition to the low-lying singlet states, carotenoids possess low-lying triplet states capable of trapping Chl *a* triplet states and quenching active oxygen species.[14] This work

* Author for correspondence. E-mail: frank@uconnvm.uconn.edu.
[†] University of Connecticut.
[‡] Marquarie University.
[§] Argonne National Laboratory.
[⊥] Northwestern University.

10.1021/jp983943f CCC: $18.00
Published on Web 01/30/1999

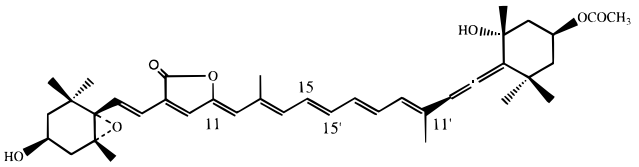

Figure 1. Structure of peridinin.

explores the dynamics of the quenching of Chl *a* triplet states by the peridinin molecules in the PCP complex.

A significant body of work has been reported using spectroscopic methodologies to elucidate the topography and binding environment of peridinin and Chl *a* in the PCP complex from *Amphidinium carterae* and related species.[8,15] The geometric requirements for energy transfer derived from this previous work have been brought into clearer focus with the presentation of the high-resolution (2.0 Å) X-ray structure of the PCP complex[6] which revealed that a noncrystallographic trimer of polypeptides comprises the fundamental light-harvesting unit. Each of these polypeptide members has pseudo 2-fold symmetry and binds eight peridinin molecules and two Chl *a* molecules. Close association, essentially van der Waals contact, exists between the peridinins and Chl *a* molecules in the complex. In the present work, data from steady-state absorption, fluorescence, fluorescence excitation, and fast transient optical spectroscopic methods are presented and discussed within the framework of the molecular structure of the complex. This paper augments the previous excellent reports of optical[16−21] and magnetic resonance[22] properties of peridinin and the PCP complex already presented. The present work (1) presents strong evidence that the primary mechanism of energy transfer is via the S_1 state of peridinin; (2) demonstrates that the triplet states of Chl *a* are quenched efficiently by the bound peridinin molecules; and (3) explores the controlling factors for energy transfer involving excited electronic states coupled to spin-forbidden and symmetry-forbidden transitions.

Materials and Methods

Sample Preparation. The PCP complex was prepared as in Sharples *et al.*[23] Pigments were extracted fom PCP by the procedure of Martinson and Plumley[24] except that 1-butanol was used in place of 2-butanol. Peridinin was separated from Chl *a* by HPLC on a C18 Econosil column (Alltech) using a two-solvent gradient. Solvent B was 50% methanol/50% acetonitrile and solvent A, 50% water/50% solvent B. The column was equilibrated with 80% A. The sample was applied at a flow rate of 2 mL/min, after 5 min a gradient to 90% B over 10 min, followed by a gradient to 99% over 5 min and then held at 99%. The eluent was monitored at 440 nm and the fractions containing peridinin dried under vacuum in darkness.

Spectroscopic Methods. *Steady-State Absorption and Fluorescence.* Absorption spectra were recorded at room temperature using a Milton Roy Spectronic 3000 Array photodiode array spectrometer. Fluorescence spectroscopy was carried out using an SLM Instruments, Inc. model 8000C spectrofluorimeter employing a 450 W ozone-free xenon arc lamp and a 1500 grooves/mm grating monochromator for excitation. The sample emission passed through a 10 mm Glan-Thompson calcite prism type polarizer and a 450 nm cutoff filter into another monochromator positioned 90° to the excitation beam. The spectral profile of the incident light and the emission were detected by two independent Hamamatsu model R-928 photomultiplier tubes. Contributions resulting from Raman scattering bands of the solvent were removed from the spectra by subtracting a solvent blank taken under identical conditions. The fluorescence spectra were also corrected for the wavelength dependences of the optical components using a correction factor generated by a Spectral Irradiance 45 W quartz−halogen tungsten coiled filament lamp standard.

Time-Resolved Optical Spectroscopy. Two different transient optical spectrometers were used. One has time resolution to 7 ns and the other has time resolution to 140 fs. For the nanosecond experiments, 40 μL of a degassed solution of PCP ($OD_{480} = 3$ in a 1 cm path) was transferred to a 2 mm path square quartz cuvette using an airtight syringe. The measuring beam was obtained from a 150 W Xe lamp passed through a 4 mm diameter aperture, a 450 nm cutoff filter, and a 20% transmitting neutral-density filter. The measuring light was then passed through the sample cuvette and the transmitted light was detected using an Instrument SA model LH20 monochromator employing a grating with 1200 grooves/mm and an RCA R928 photomultiplier. The output signal was amplified by a Stanford Research System model SR445 amplifier. A Tektronix oscilloscope model TDS 620A was used for signal averaging. Each transient profile consisted of 1000 points per trace and was recorded as an average of 1000 scans. The intensity of the probe light was 4 mW. A Quanta-Ray DCR-3/PDL-2 Nd:YAG-pumped dye laser having a pulse duration of 7 ns at 580 nm using Rhodamine 610 in spectroscopic grade methanol was employed at a pulse repetition rate of 20 Hz. The laser beam was aligned perpendicular to the probe beam and focused onto the sample. The flash laser intensity was kept in the region where the amplitudes of the transient signals increased linearly with flash intensity.

The transient absorption apparatus used to measure the subpicosecond excited state lifetimes consisted of a homemade, self-mode-locked, Ti:sapphire oscillator that was pumped by the 3 W output from a Spectra Physics Millennia CW frequency-doubled, diode-pumped ND:YAG laser.[25] The Ti:sapphire oscillator emits 25 fs, 840 nm pulses which were temporally stretched using a double-passed grating/mirror combination to a duration of ca. 200 ps. The chirped pulses were amplified with a homemade Ti:sapphire regenerative amplifier that employed a folded cavity, and used a double-step Pockels cell (Medox)/thin film polarizer combination for injection and cavity dumping. The regenerative amplifier was pumped by an intracavity frequency-doubled, Q-switched, ND:YAG laser (Spectra Physics 3450) that produced 3.8 mJ, 50 ns, 532 nm pulses at a 1.27 kHz repetition rate. The output of the Ti:sapphire regenerative amplifier was recompressed with 70% efficiency using a grating pair to give 200 μJ, 140 fs, 840 nm pulses at a 1.27 kHz repetition rate. Using appropriate beamsplitters, about 10 μJ of 840 nm light was used to generate a very smooth white light continuum by focusing it with a 5 cm lens into a 2 mm thick sapphire window. Shot-to-shot intensity fluctuations of the probe beam were generally less than 5%. The remaining 840 nm was frequency doubled with 35% efficiency by using a 2 mm long type I LBO crystal to yield 140 fs, 420 nm pulses.

The 420 nm light was used to pump a two-stage optical parametric amplifier[26] that furnished 140 fs transform limited pulses that were tunable from 470 to 820 nm with energies up to 5 μJ per pulse. The energy of the excitation light on the sample was controlled using a polarizer−$^1/_2$ in. waveplate combination. Typically 0.3−1 μJ was used to excite the molecules. The excitation beam was synchronously chopped at one-half the laser repetition rate. The white light probe beam was split into measuring and reference beams. The arrival of the pump beam relative to the measuring probe beam was

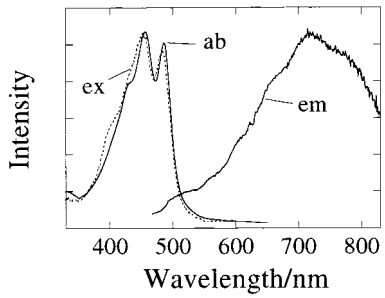

Figure 2. Absorbance (ab), fluorescence (em), and fluorescence excitation (ex) spectra of peridinin in *n*-hexane at room temperature. The vertical scale is arbitrary. The spectra were all normalized to their peak maxima.

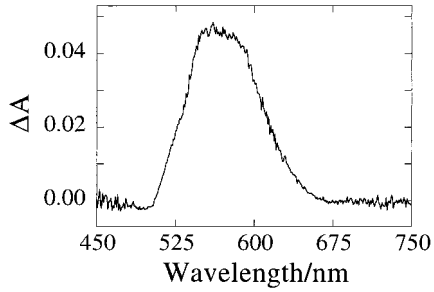

Figure 3. $S_1 \rightarrow S_n$ spectrum of peridinin in methanol at room temperature after excitation by a 140 fs laser pulse at 500 nm.

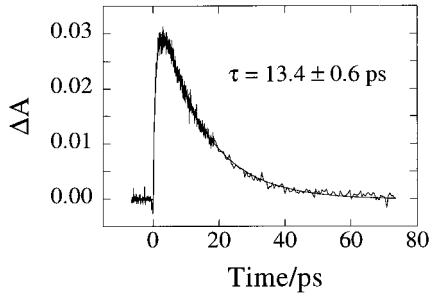

Figure 4. Decay of the $S_1 \rightarrow S_n$ transition of peridinin in methanol at room temperature after excitation by a 140 fs laser pulse at 500 nm with the probe wavelength set at 560 nm. The decay corresponds to the S_1 lifetime of peridinin.

accomplished with an optical delay line that used a linear stepping motor (Compumotor) with 1 μm (6.6 fs) resolution. The nearly-collinear and codirectional excitation and measuring probe beams were focused into the sample to a 0.3 mm diameter spot size. The carotenoid was dissolved in methanol and was placed in a 2 mm path length cuvette. Following deoxygenation of the sample by bubbling with nitrogen gas, the cuvettes were sealed. The wavelength of the measuring and reference probe beams were selected with a computer-controlled monochromator (ISA/SPEX M270). Changes in the transmission of the measuring probe light through the sample and changes in the reference probe beam were monitored by photodiodes. The output of each photodiode was integrated by a gated integrator (Evans), and both signals were digitized and recorded by a personal computer (Gateway P6-200). The data acquisition software monitored the quality of each shot and only averaged shots within 5% of the average intensity of the reference probe beam level. Kinetic parameters were obtained by iterative reconvolution using the Levenberg−Marquardt algorithm. The instrumental time response was 140 fs at 420 nm.

Results and Discussion

Peridinin in Solution. Figure 2 shows the room temperature absorbance, fluorescence, and fluorescence excitation spectra of peridinin in *n*-hexane. The absorbance spectrum is characterized by an intense band having a maximum at 456 nm, known to be associated with the $S_0 \rightarrow S_2$ ($1^1A_g \rightarrow 1^1B_u$) transition. The longest wavelength vibronic feature in the spectrum corresponds to the spectral origin and is located at 486 nm. From this observation, the energy of the S_2 state relative to the ground state of peridinin in *n*-hexane can be determined to be 20 600 $\pm$ 100 cm^{-1}. The fluorescence spectrum of peridinin in *n*-hexane has a maximum at 720 nm, which is 264 nm to the red of the maximum of its absorption spectrum (Figure 2). This large red shift between the emission and absorption suggests that the fluorescence emission from peridinin corresponds to an $S_1 \rightarrow S_0$ ($2^1A_g \rightarrow 1^1A_g$) transition rather than an $S_2 \rightarrow S_0$ ($1^1B_u \rightarrow 1^1A_g$) transition. This may be observed if internal conversion from the S_2 state to the S_1 state occurs with a higher probability than fluorescence from the S_2 state. Carotenoids having less than nine carbon−carbon double bonds typically display this behavior.[27] As seen in Figure 2, the fluorescence excitation spectrum corresponds very well to the absorption spectrum and strongly supports the notion that the emission does indeed originate from peridinin. However, the spectral origin for the emission is difficult to determine owing to the lack of vibronic features in the band profile, although noticeable inflections are apparent in the spectrum (Figure 2). (See also Figure 1E in Mimuro *et al.*[17] for the spectrum in CS_2.) Cosgrove *et al.*[28] provided insight into how one might assign the origins of emission of polyenes whose spectra lack resolution in their vibronic features. These authors compared the high-resolution emission spectrum of all-*trans*-2,4,6,8,10,12,14-hexadecaheptaene with the less-resolved spectrum of all-*trans*-β-apo-12′-carotenal at 77 K (see Figure 4 in Cosgrove *et al.*[28]), and demonstrated that the spectral origins of these two homologous π-electron systems lie roughly 2750 cm^{-1} to the blue of the position of maximum emission, or in other words, at the second vibronic feature to higher energy relative to the Franck−Condon maximum. If one applies this logic to peridinin in solution, the spectral origin of the $S_1 \rightarrow S_0$ ($2^1A_g \rightarrow 1^1A_g$) emission profile would be at ~600 nm, corresponding to a transition energy of ~16 700 cm^{-1}.

For the measurement of the excited singlet state lifetimes, peridinin was dissolved in methanol where it displays an absorption spectrum at the same λ_{max} (~475 nm) as that of peridinin in the PCP complex. The sample was excited at 500 nm with a 140 fs laser pulse and resulted in a rapid, instrument-limited buildup of an $S_1 \rightarrow S_n$ absorption band having a width of ~175 nm and a maximum at ~560 nm (Figure 3). The decay of this absorption band occurs with single-exponential kinetics corresponding to a lifetime of 13.4 $\pm$ 0.6 ps (Figure 4). Comparing this value of the S_1 state decay time to the lifetimes of several carotenoids whose $S_1 \rightarrow S_0$ ($2^1A_g \rightarrow 1^1A_g$) transition energies are known from fluorescence studies,,[27,29,30] a value of 13.4 $\pm$ 0.6 ps would appear to be too short to correspond to a transition energy of ~16 700 cm^{-1}. From a comparison with the dynamics of several other carotenoids and based on the energy gap law of Englman and Jortner,[31] the value for the $S_1 \rightarrow S_0$ ($2^1A_g \rightarrow 1^1A_g$) transition energy of peridinin that would be more consistent with a 13.4 $\pm$ 0.6 ps lifetime is 14 600 $\pm$ 50 cm^{-1}. However, this is not in agreement with the ~16 700 cm^{-1} assignment of the $S_1 \rightarrow S_0$ ($2^1A_g \rightarrow 1^1A_g$) transition energy based on the analysis of the features of the $S_1 \rightarrow S_0$ ($2^1A_g \rightarrow 1^1A_g$) emission spectrum described above. The question that remains is, why is the peridinin S_1 lifetime in methanol shorter

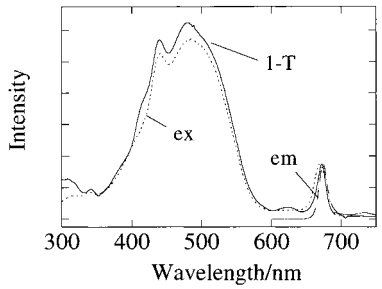

Figure 5. Fluorescence (em), fluorescence excitation (ex), and 1-*T* spectra, where *T* is the transmittance, of the PCP complex at room temperature. The emission and excitation spectra were normalized to the 1-*T* maximum peak intensity of Chl at 672 nm.

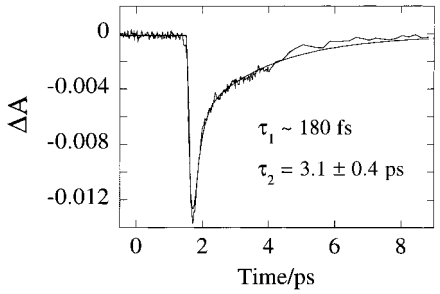

Figure 6. Kinetic trace associated with the bleaching and recovery dynamics of the peridinin absorption in the PCP complex after excitation by a 140 fs laser pulse at 530 nm and the probe wavelength set at 550 nm at room temperature. An instantaneous onset of bleaching was followed by a two-component recovery of the transient. One of these components was ~180 fs and accounted for ~70% of the signal, whereas the other corresponded to a lifetime of 3.1 ± 0.4 ps and accounted for ~30% of the signal.

than expected based on the energy gap law? The answer probably lies in that fact that the peridinin molecule is highly substituted compared to most other carotenoids. It has an allene moiety and a lactone ring both of which are connected directly to its π-electron conjugated system (Figure 1). The combined presence of these substituents may lead to unique dynamics behavior of peridinin compared to other carotenoids. In particular, the presence of a carbonyl group in the conjugated chain has been shown to affect the origin of fluorescence.[19] Neoxanthin, which lacks the lactone ring, but is otherwise similar in its structure to peridinin fluoresces predominantly from its S_2 state. Fucoxanthin, which has a carbonyl functional group but not the lactone ring, emits predominantly from its S_1 state like peridinin.[17] Katoh *et al.*[16] suggested that a distortion in the configuration of the carotenoid owing to the presence of the carbonyl group may be responsible for the effect on the origin of the fluorescence. A change in the displacement of the potential surface of the S_1 state relative to that of the S_2 state, that enhances S_2 to S_1 internal conversion, may favor $S_1 \rightarrow S_0$ ($2^1A_g \rightarrow 1^1A_g$) emission over $S_2 \rightarrow S_0$ ($1^1B_u \rightarrow 1^1A_g$) emission. However, the coupling of nπ* states derived from the carbonyl functional group to S_1 and S_2 may affect the dynamics of the S_1 state of peridinin and cannot yet be ruled out.

Peridinin in the PCP Complex. The fluorescence, fluorescence excitation, and 1-*T* spectra, where *T* is the transmittance, of the PCP complex were taken at room temperature and are shown in Figure 5. The maximum in the 1-*T* spectrum of peridinin is located at 488 nm. A noticeable shoulder corresponding to the Soret absorption band of Chl *a* is observed at 440 nm. The Q_y transition of Chl *a* is observed at 672 nm. Fluorescence from Chl *a* is observed upon excitation into the peridinin absorption region. The Chl *a* fluorescence has a maximum peak at 674 nm. If one normalizes the intensity of the fluorescence excitation spectrum to the 1-T spectrum at 672 nm, the efficiency of singlet energy transfer from peridinin to Chl *a*, based on the intensity of the peridinin peak at 488 nm, is calculated to be 88 ± 2%.

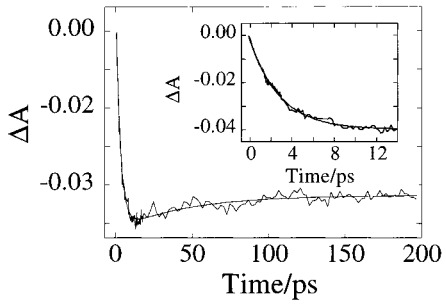

Figure 7. Onset of Chl *a* bleaching and subsequent decay probed at the Chl *a* Q_y absorption band at 670 nm after excitation by the pump laser at 530 nm in the carotenoid region at room temperature. The full trace shows the rise of Chl *a* bleaching in 3.2 ± 0.3 ps followed by 2 decay phases corresponding to lifetimes of 46 ± 5 ps and 4.5 ± 0.1 ns. The inset shows that the rise of the signal is well-fit by a single-exponential function. No evidence for a contribution from a subpicosecond component is seen.

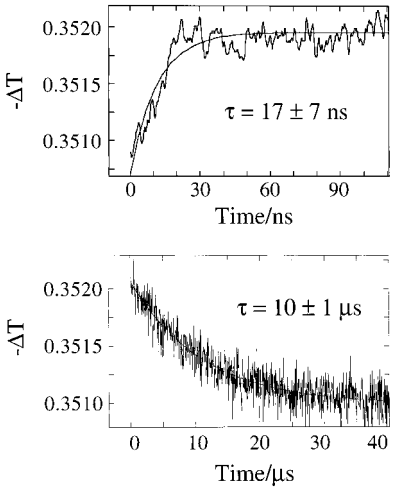

Figure 8. Rise and decay profiles at room temperature of the triplet−triplet absorption signals observed in the PCP complex after excitation at 580 nm and probing at 555 nm. Both the rise and decay curves were best fit by single exponentials. The dynamics of the peridinin triplet state in the PCP complex was determined to be 17 ± 7 ns for the rise and 10 ± 1 μs for the decay.

For the measurement of the excited singlet state dynamics of peridinin in the PCP complex, the protein was excited by a pump laser into the carotenoid absorption region at 530 nm. With the probe laser tuned to 550 nm in the carotenoid absorption region, after excitation with the pump laser, there was an instantaneous onset of bleaching followed by a two-component recovery of the transient (Figure 6). One of these components was approximately 180 fs and accounted for ~70% of the signal. The other corresponded to a lifetime of 3.1 ± 0.4 ps and accounted for ~30% of the signal (Figure 6). When the probe laser was tuned to the Chl *a* Q_y absorption band at 670 nm, after excitation by the pump laser at 530 nm in the carotenoid region, the dynamics showed an onset of Chl *a* bleaching in 3.2 ± 0.3 ps followed by two decay phases corresponding to lifetimes of 46 ± 5 ps and 4.5 ± 0.1 ns (Figure 7). The inset of Figure 7 shows that the rise of this signal is well fit by a single-exponential function. No evidence for a contribution from a subpicosecond component is seen.

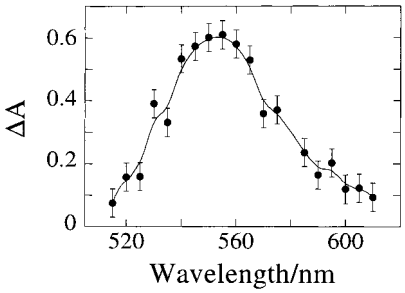

Figure 9. Triplet−triplet absorption spectrum of peridinin in the PCP complex measured after excitation at 580 nm at room temperature. The vertical axes are in arbitrary units and represent negative changes in transmission monitored at 555 nm.

The interpretation of these results is as follows: The ∼180 fs decay component seen while probing the carotenoid absorption region at 550 nm is associated with the internal conversion of S_2 to S_1 of peridinin. A similar value of 192 ± 7 fs for this molecule has been reported[21] and assigned as the S_2 lifetime. In this time domain at 550 nm an $S_1 \rightarrow S_n$ transition for peridinin is expected to build up (Figure 3). However, the S_1 state of peridinin is depopulated in 3.1 ps by a combination of internal conversion to the ground state which occurs in 13.4 ps in methanol (Figure 4), and energy transfer to Chl. The 3.2 ps rise of the Chl *a* bleaching at 670 nm (inset of Figure 7) is associated with the peridinin-to-Chl *a* singlet state energy transfer time, $1/k_{ET}$. The 46 ps decay component probably corresponds to a small amount of singlet annihilation commonly seen in laser pump−probe experiments on antenna complexes.[32] The 4.5 ns decay component corresponds to the Chl *a* singlet lifetime in the PCP complex.

Using the equation, $\epsilon = k_{ET}/(k_{ET} + k_{ic})$, where ϵ is the energy transfer efficiency, and $1/k_{ET} = 3.2 \pm 0.3$ ps for the S_1 decay in the PCP complex, and $1/k_{ic} = 13.4 \pm 0.6$ ps for the S_1 dynamics of peridinin measured in methanol solution, a value of 82 ± 14% for the energy transfer efficiency is obtained. This is within the experimental error of the 88 ± 2% value measured here using steady-state fluorescence excitation spectroscopy (Figure 5). The facts that (i) the 3.1 ps decay of the S_1 state of peridinin in the complex is only slightly faster than the 3.2 ps onset of the Chl *a* bleaching; (ii) the energy transfer efficiency can be accounted for solely on the basis of the behavior of the S_1 state of peridinin; and (iii) there is no evidence for a subpicosecond component in the rise of the Chl *a* bleaching at 670 nm (Figure 7) lend strong support to the idea that the mechanism of energy transfer from peridinin to Chl *a* occurs primarily through the S_1 state of the carotenoid. It may be noted that the lifetime of the peridinin S_1 state has been measured to be 103 ps in CS_2.[21] If the S_1 lifetime of peridinin in a protein environment were of this order, the efficiency would be ∼100% rather than 88% measured here. Moreover, the spectral origin of absorption and spectroscopic features of peridinin in CS_2 are significantly different from those for peridinin in the PCP complex. Further investigation of the S_1 lifetime of peridinin in different solvent environments is clearly required.

Figure 8a,b shows the rise and decay profiles at room temperature of the triplet−triplet absorption signals of the PCP complex. Both the rise and decay curves were best fit by single exponentials. The dynamics of the peridinin triplet state in the PCP complex was determined to be 17 ± 7 ns for the rise and 10 ± 1 μs for the decay. The amplitudes of the transients plotted versus wavelength (Figure 9) display a spectral maximum at 555 nm. These results are typical of triplet spectra and triplet energy transfer times involving carotenoids and Chls.[33,34]

Because the structure the PCP complex has been solved to 2 Å resolution, it is interesting to seek a correlation between specific molecules in the protein and the mechanisms of singlet and triplet state energy transfer. As mentioned above, the minimal unit of the PCP complex consists of a trimer of protein subunits. Each of the individual protein subunits comprising the trimer binds two molecules of Chl *a* and eight molecules of peridinin (Figure 10). One Chl *a* molecule is surrounded by four peridinins and is related to the other Chl *a* molecule and its associated four peridinins by a pseudo C_2 symmetry axis. There is van der Waals contact between pairs of peridinins and between the peridinins and the Chl *a* molecule. The distance between pairs of peridinins is approximately 8−11 Å. All four peridinin molecules in a group have very similar distances of closest approach of their π-electron conjugated chains to the π-electron conjugation of their respective Chls with values ranging from 3.70 to 5.00 Å. (See Table 1.) In contrast, one specific peridinin out of four in each group has a much closer

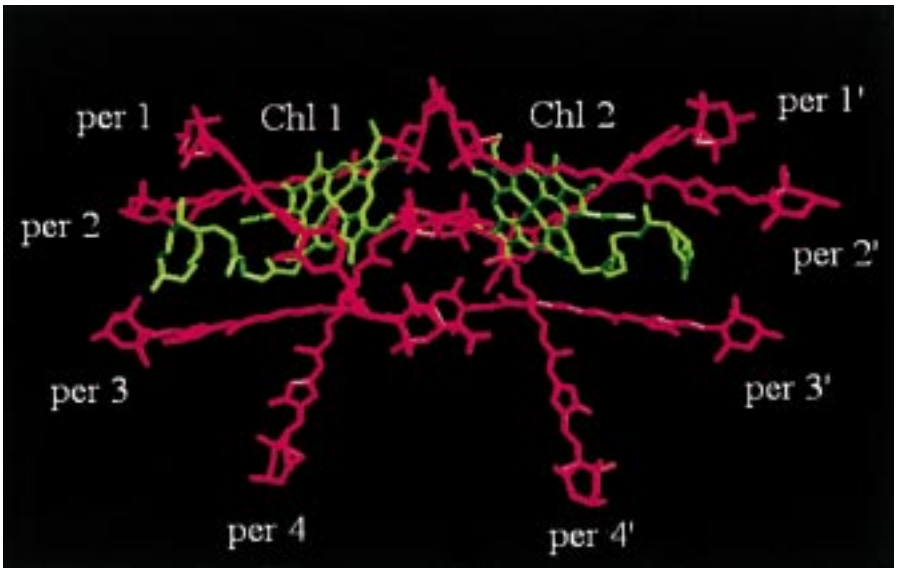

Figure 10. Structure of the pigments associated with one-third of the trimeric minimal unit comprising the PCP complex. A pseudo 2-fold axis runs vertically in the center of the picture. Structure taken from coordinates of the PCP complex 1PPR deposited in the Brookhaven Protein Data Bank by Hofmann et al.[6]

TABLE 1: Distances and Cosine Projections of the Chl *a* and Peridinin (per) Molecules[a]

	distance (Å) of closest approach of π-electron systems	center-to-center distance (Å) between pigments	projection of Chl Q_x onto carotenoid long axis	projection of Chl Q_y onto carotenoid long axis
Chl and per 1/1′	5.00/4.71	5.44/5.36	0.103/0.0918	−0.992/−0.988
Chl and per 2/2′	4.24/4.14	9.36/9.49	0.790/0.766	−0.467/−0.515
Chl and per 3/3′	4.38/4.50	8.57/8.57	0.769/0.726	−0.537/−0.582
Chl and per 4/4′	4.24/3.70	8.97/8.97	0.973/0.953	0.134/0.164

[a] The distance of closest approach of the π-electron conjugated systems was measured from an outside edge of the chlorophyll conjugation to the closest point in the π-electron conjugated system along the carbon chain of the carotenoid. The center-to-center distance was measured from the Mg center of the Chl to carbon 15 in the peridinin (Figure 1). The long axis of a peridinin is defined as a vector connecting carbons 11 and 11′ in the carotenoid. The two numbers in each cell of the table represent the distances and projections corresponding to the two groups of single Chls and four peridinins related by the pseudo C_2 symmetry axis.

center-to-center distance than the other three in the same group. (See per 1 and per 1′ in Table 1.) Also, this specific peridinin has, by far, the largest projection of its long axis onto the Q_y transition moment axis of the Chl. (See Table 1.) As shown above, singlet energy transfer from the peridinin to Chl *a* involves the S_1 state of the carotenoid as the donor state. This state is associated with the $S_1 \rightarrow S_0$ ($2^1A_g \rightarrow 1^1A_g$) transition which has a vanishingly small transition dipole moment. Because of this, singlet energy transfer does not involve dipolar interactions. It has been suggested that the mechanism of singlet energy transfer involves higher order multipolar interactions[35] or exchange interactions,[36] the latter of which decreases exponentially with intermolecular separation.[37] The very close proximity of peridinins, per 1 and per 1′, to their respective Chl *a* molecules, the alignment of the π-electron systems, and the significant spectral overlap between the $S_1 \rightarrow S_0$ ($2^1A_g \rightarrow 1^1A_g$) emission and the Chl *a* Q_y absorption (see Figures 2 and 5, respectively) would satisfy more than any of the other peridinins, the stringent distance, orbital overlap, and energy requirements for singlet energy transfer between the carotenoid and Chl.

Interestingly, per 4 and per 4′ have large projections of their long axes onto their respective Chl Q_x transition moments. (See Table 1.) The peridinin-to-Chl center-to-center distance is not as close as for per 1 and per 1′, however, and the spectral overlap between the $S_1 \rightarrow S_0$ ($2^1A_g \rightarrow 1^1A_g$) emission and the Q_x absorption which occurs at ~620 nm (Figure 5) is not as significant as that between the carotenoid S_1 emission and the Q_y transition. However, singlet energy transfer involving the $S_1 \rightarrow S_0$ ($2^1A_g \rightarrow 1^1A_g$) transition of peridinin and the Q_x transition of Chl is quite likely, especially for per 4 and per 4′. A mechanism involving the Q_x transition of BChl has been invoked by Desamero *et al.*[38] to explain singlet energy transfer between carotenoids and BChl in LHII complexes incorporated with spheroidene analogues having different π-electron conjugated chain lengths.

Triplet energy transfer involves the T_1 state of the carotenoid and has a vanishingly small transition dipole moment associated with its spin-forbidden $S_0 \rightarrow T_1$ transition. Because of this, triplet energy transfer, analogous to singlet energy transfer involving the S_1 state of peridinin, has a very stringent distance requirement. Close proximity, essentially van der Waals contact between pigments, is required for efficient transfer. Triplet energy transfer also requires that a triplet state of sufficiently low energy exists on the energy acceptor. The distance requirement is satisfied by per 1 and per 1′ more than any of the other peridinins, making these the most likely energy traps for any Chl triplet states that are formed.

The data presented in this study show that the primary route of energy transfer from peridinin to chlorophyll in the PCP complex is through the S_1 state of peridinin. Close association between the peridinins and chlorophylls, clearly evident in the 3-D structure of the PCP complex, along with proper alignment of pigments and the energy state matching are responsible for the high efficiencies of the singlet and triplet energy transfer processes.

Acknowledgment. The authors thank Professor Ronald Christensen for useful discussions and Karissa Atticks for technical assistance. This work was supported by grants to H.A.F. from the National Institutes of Health (GM-30353) and the University of Connecticut Research Foundation. The work at Argonne National Laboratory was supported by the Office of Basic Energy Sciences, Division of Chemical Sciences, U.S. Department of Energy, under Contract W-31-109-Eng-38.

References and Notes

(1) Blankenship, R. E., Ed. In *Anoxygenic Photosynthetic Bacteria*, *Advances in Photosynthesis*, Kluwer Academic Publishing: New York, 1995.

(2) McDermott, G.; Prince, S. M.; Freer, A. A.; Hawthornthwaite-Lawless, A. M.; Papiz, M. Z.; Cogdell, R. J.; Isaacs, N. W. *Nature* **1995**, *374*, 517.

(3) Koepke, J.; Hu, X.; Muenke,.K.; Schulten, K.; Michel, H. *Structure* **1996**, *4*, 581.

(4) Kuhlbrandt, W.; Wang, D. N.; Fujiyoshi, Y. *Nature* **1994**, *367*, 614.

(5) Matthews, B. W.; Fenna, R. E.; Bolognesi, M. C.; Schmid, M. F.; Olsen, J. M. *J. Mol. Biol.* **1979**, *181*, 259.

(6) Hofmann, E.; Wrench, P.; Diedrichs, K.; Sharples, F. P.; Hiller, R. G.; Welte, W.; Diedrichs, K. *Science* **1996**, *272*, 1788.

(7) Siefermann-Harms, D. *Photochem. Photobiol.* **1982**, *35*, 719.

(8) Song, P.; Koka, P.; Prezelin, B.; Haxo, F. *Biochemistry* **1976**, *15*, 4422.

(9) Frank et al., unpublished results

(10) Angerhofer, A.; Cogdell, R. J.; Hipkins, M. F. *Biochim. Biophys. Acta* **1986**, *848*, 333.

(11) Hudson, B. S.; Kohler, B. E.; Schulten, K. In *Excited States*; Lim, E. C., Ed.; Academic Press: New York, 1982; Vol. 6, p 2.

(12) Hudson, B. S.; Kohler, B. E. *Synth. Met.* **1984**, *9*, 241.

(13) Cogdell, R. J.; Frank, H. A. *Biochim. Biophys. Acta* **1987**, *895*, 63.

(14) Frank, H. A.; Cogdell, R. J. *Photochem. Photobiol.* **1996**, *63*, 257.

(15) Koka, P.; Song, P. *Biochim. Biophys. Acta* **1977**, *495*, 220.

(16) Katoh, T.; Nagashima, U.; Mimuro, M. *Photosynth. Res.* **1991**, *27*, 221.

(17) Mimuro, M.; Nagashima, U.; Takaichi, S.; Nishimura, Y.; Yamazaki, I.; Katoh, T. *Biochim. Biophys. Acta* **1992**, *1098*, 271.

(18) Mimuro, M.; Katoh, T. *Pure and Appl. Chem.* **1991**, *63*, 123.

(19) Mimuro, M.; Nishimura, Y.; Takaichi, S.; Yamano, Y.; Ito, M.; Nagaoka, S.; Yamazaki, I.; Katoh, T.; Nagashima, U. *Chem. Phys. Lett.* **1993**, *213*, 576.

(20) Ogata, T.; Kodama, M.; Nomura, S.; Kobayashi, M.; Nozawa, T.; Katoh, T.; Mimuro M. *FEBS Lett.* **1994**, *356*, 367.

(21) Akimoto, S.; Takaichi, S.; Ogata, T.; Nishimura, Y.; Yamazaki, I.; Mimuro, M. *Chem. Phys. Lett.* **1996**, *260*, 147.

(22) Carbonera, D.; Giacometti, G.; Segre, U. *J. Chem. Soc., Faraday Trans.* **1996**, *92*, 989.

(23) Sharples, F. P.; Wrench, P. M.; Ou, K.; Hiller, R. G. *Biochim. Biophys. Acta* **1996**, *1276*, 117.

(24) Martinson, T. A.; Plumley, G. F. *Anal. Biochem.* **1995**, *228*, 123.
(25) Gosztola, D.; Yamada, H.; Wasielewski, M. R. *J. Am. Chem. Soc.* **1995**, *117*, 2041.
(26) Greenfield, S. R.; Wasielewski, M. R. *Opt. Lett.* **1995**, *20*, 1394.
(27) Frank, H. A.; Desamero, R. Z. B.; Chynwat, V.; Gebhard, R.; van der Hoef, I.; Jansen, F. J.; Lugtenburg, J.; Gosztola, D.; Wasielewski, M. R. *J. Phys. Chem.* **1997**, *101*, 1, 149.
(28) Cosgrove, S. A.; Guite, M. A.; Burnell, T. B.; Christensen, R. L. *J. Phys. Chem.* **1990**, *94*, 8118.
(29) Frank, H. A.; Farhoosh, R.; Gebhard, R.; Lugtenburg, J.; Gosztola, D.; Wasielewski, M. R. *Chem. Phys. Lett.* **1993**, *207*, 88.
(30) Chynwat, V.; Frank, H. A. *Chem. Phys.* **1995**, *194*:, 237.
(31) Engelman, R.; Jortner J. *Mol. Phys.* **1970**, *18*, 145.
(32) Trautman, J. K.; Shreve, A. P.; Violette, C. A.; Frank, H. A.; Owens, T. G.; Albrecht, A. C. *Proc. Natl. Acad. Sci. U.S.A.* **1990**, *87*, 215.
(33) Frank, H. A. In *The Photosynthetic Reaction Center*; Norris, J. R., Deisenhofer J., Eds.; Academic Press: New York, 1993; Vol. 2.
(34) Frank, H. A.; Cogdell, R. J. *Photochem. Photobiol.* **1996**, *63*, 257.
(35) Nagae, H.; Kikitani, T.; Katoh, T.; Mimuro, M. *J. Chem. Phys.* **1993**, *98*, 8012.
(36) Naqvi, K. R. *Photochem. Photobiol.* **1980**, *31*, 523.
(37) Dexter, D. L. *J. Chem. Phys.* **1953**, *21*, 836.
(38) Desamero, R. Z. B.; Chynwat, V.; van der Hoef, I.; Jansen, F. J.; Lugtenburg, J.; Gosztola, D.; Wasielewski M. R.; Cua, A.; Bocian, D. F.; Frank, H. A. *J. Phys. Chem.* **1938**, *42*, 8151.